RESEARCH ARTICLE

Figures and figure supplements

Shank promotes action potential repolarization by recruiting BK channels to calcium microdomains

Luna Gao *et al*

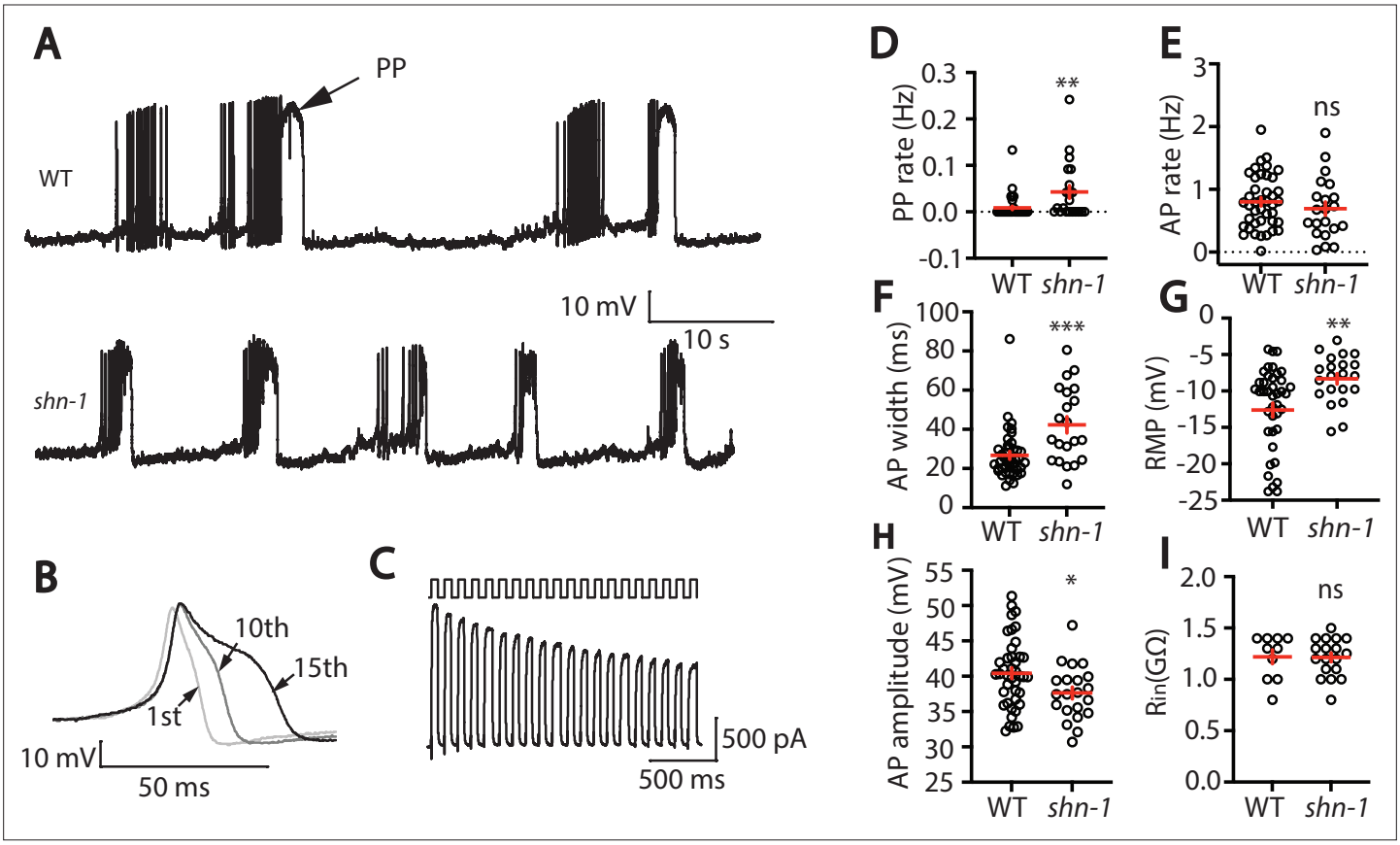

Figure 1. SHN-1 regulates muscle AP firing patterns. (**A**) Representative traces of spontaneous muscle APs are shown for WT and *shn-1(nu712* null) mutants. APs occur in bursts of ~10 APs/ burst. Plateau potentials (PPs), defined as transients lasting >150ms, are observed less frequently, often at the end of a burst. (**B**) APs become progressively longer during bursts. Successive APs taken from a representative burst are shown. (**C**) Repetitive depolarization to +30 mV leads to a progressive decrease in potassium currents. A representative recording from a WT animal is shown. This likely results from an accumulation of inactivated potassium channels during repetitive stimulation. (**D–I**) Mean PP rate (**D**), AP rate (**E**), AP width (**F**), RMP (**G**), AP amplitude (**H**), and input resistance (R_{in}, **I**) are compared in WT and *shn-1* null mutants. All *shn-1* data were obtained from *shn-1(nu712)* except for R_{in} (**I**), which were from *shn-1(tm488)*. Values that differ significantly from wild type controls are indicated (ns, not significant; *, $p < 0.05$; **, $p < 0.01$; ***, $p < 0.001$). Error bars indicate SEM.

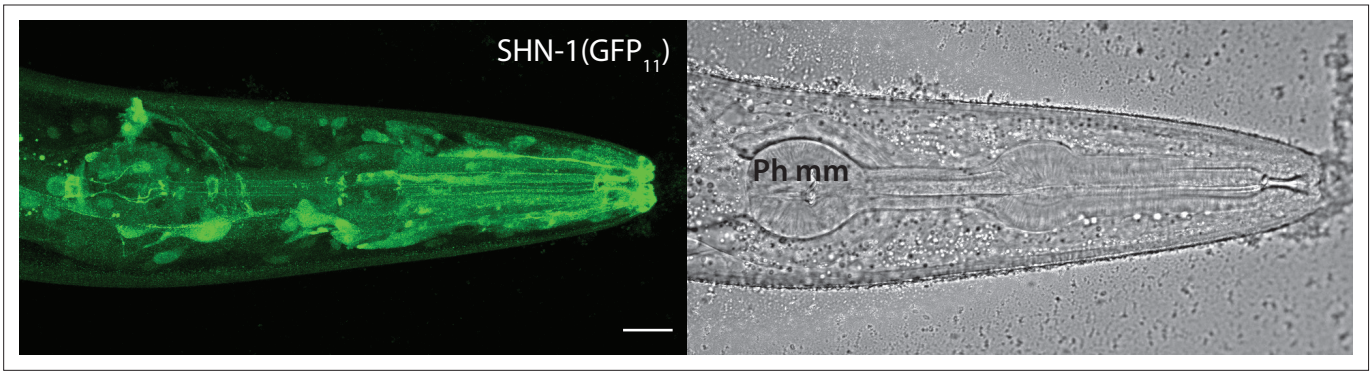

Figure 1—figure supplement 1. SHN-1 is expressed in many tissues. Endogenous SHN-1 is broadly expressed, including in neurons, muscles, skin, and glia. A representative image of reconstituted fluorescence produced by *shn-1(nu600* GFP_{11}) and eft-3>GFP_{1-10} (left) and the corresponding bright field image (right) are shown. Pharyngeal muscles (Ph mm) are indicated in the bright field image. SHN-1(GFP_{11}) expression in body muscles was not detected, consistent with the very low *shn-1* mRNA levels reported in body muscles (***Cao et al., 2017***; ***Packer et al., 2019***). Scale bar indicates 14 μm.

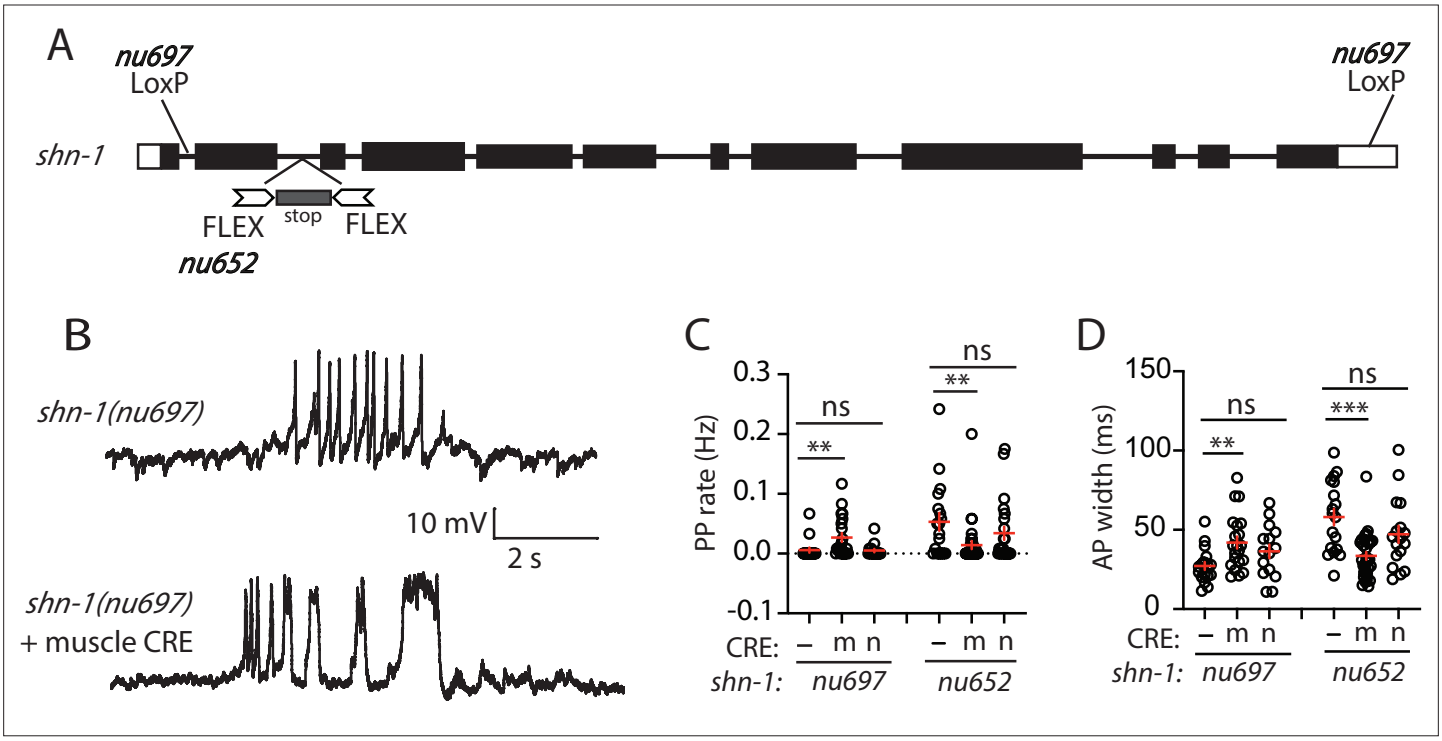

Figure 2. SHN-1 acts in muscles to control AP duration. (**A**) A schematic of the *shn-1* locus is shown. Open boxes indicate UTRs, black boxes indicate coding regions. Recombination sites mediating CRE induced deletions (LoxP) and inversions (FLEX) are indicated. The *shn-1(nu697)* allele allows CRE-induced *shn-1* knockouts while *shn-1(nu652)* allows CRE-induced *shn-1* rescue. In *shn-1(nu652)*, an exon containing in frame stop codons was inserted into the second intron (in the 'OFF' orientation). This stop exon is bounded by FLEX sites. (**B**) Representative traces of spontaneous muscle APs are shown in *shn-1(nu697)* with and without muscle CRE expression. Mean PP rate (**C**) and AP width (**D**) are compared in the indicated *shn-1* mutants without (-) and with CRE expression in muscles (**m**) or neurons (**n**). Sample sizes are as follows: *shn-1(nu697)* (17); *shn-1(nu697)* +muscle CRE (21); *shn-1(nu697)* +neuron CRE (15); *shn-1(nu652)* (18); *shn-1(nu652)* +muscle CRE (30); and *shn-1(nu652)* +neuron CRE (19). Values that differ significantly from wild-type controls are indicated (ns, not significant; *, $p < 0.05$; **, $p < 0.01$; ***, $p < 0.001$). Error bars indicate SEM. Representative traces for genotypes in panels C and D are shown in ***Figure 2—figure supplement 1***.

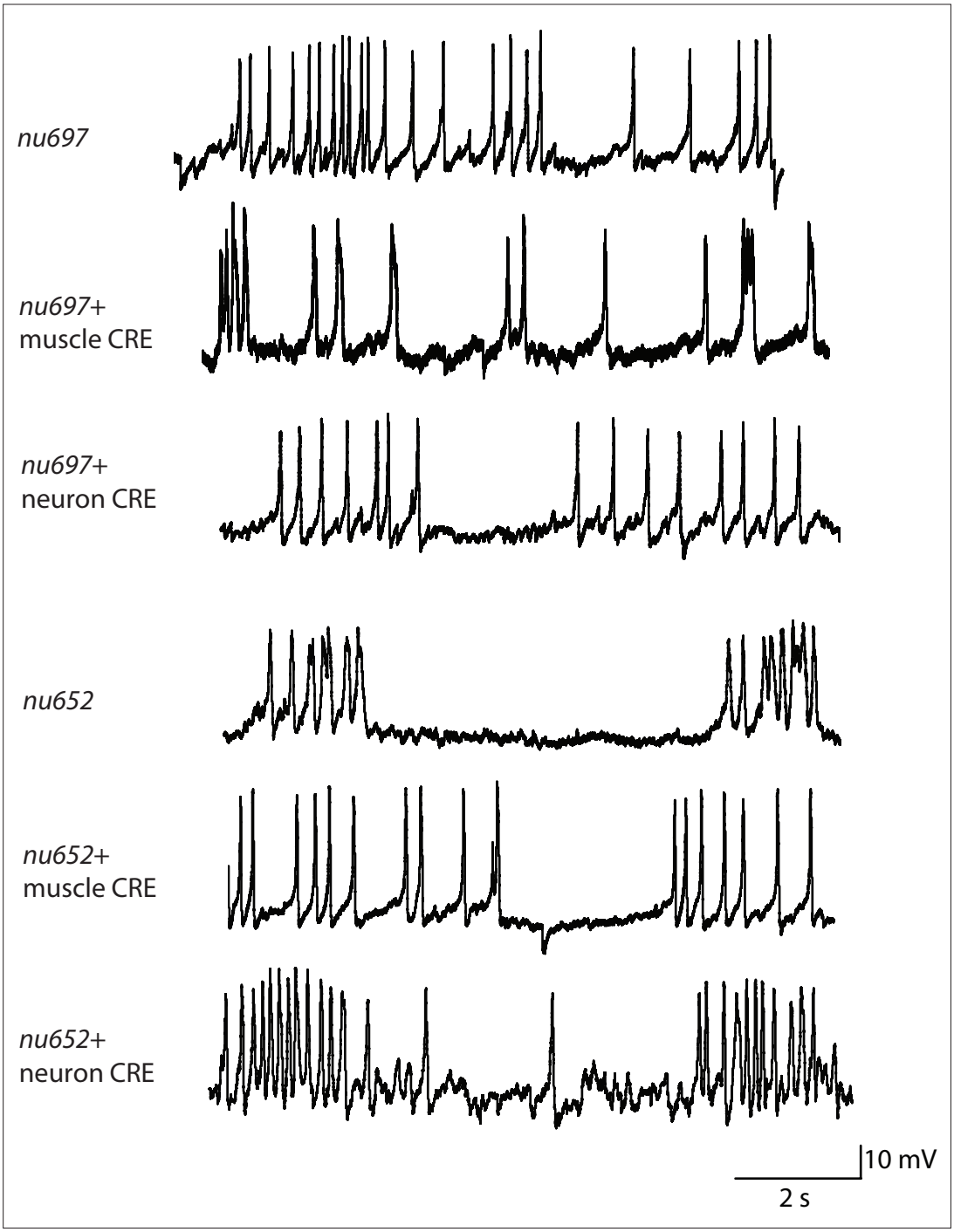

Figure 2—figure supplement 1. Representative traces for recordings summarized in ***Figure 2C and D***. Representative traces of spontaneous muscle APs are shown for the indicated genotypes.

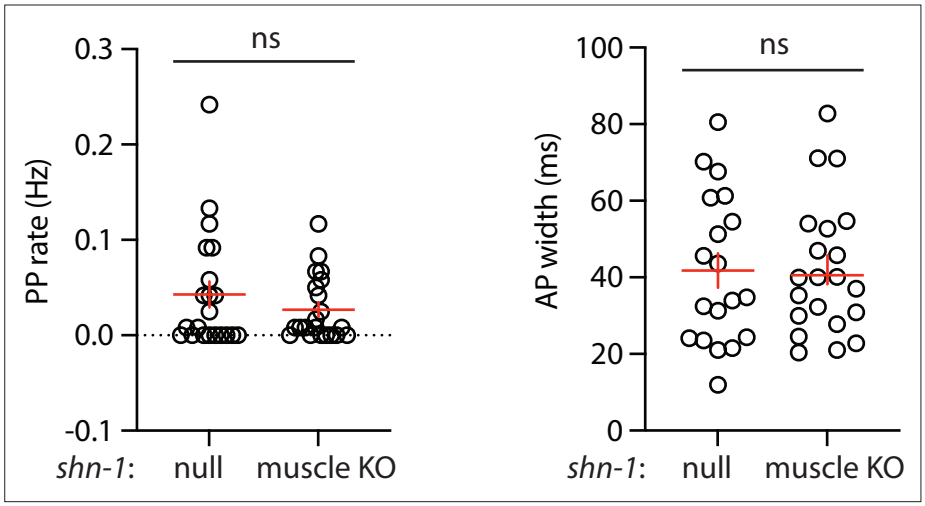

Figure 2—figure supplement 2. Muscle AP defects in *shn-1(null)* and *shn-1(muscle KO)* are not significantly different. Mean PP rate and AP width are compared in the indicated *shn-1* mutants. Sample sizes are as follows: *shn-1(nu712* null) (21); *shn-1(nu697)* +muscle CRE (21). Error bars indicate SEM. No significant differences were observed.

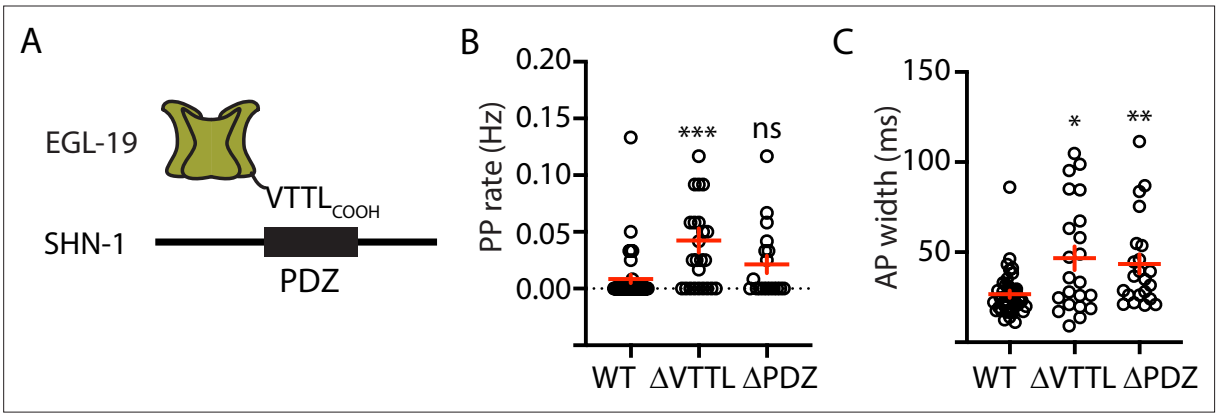

Figure 3. Mutations disrupting SHN-1 binding to EGL-19 increase AP duration. (**A**) A schematic illustrating the binding interaction between EGL-19's c-terminus and SHN-1's PDZ domain is shown. (**B–C**) Mean PP rate and AP width are compared in the indicated genotypes. Representative traces are shown in ***Figure 3—figure supplement 1***. Mutations deleting the SHN-1 PDZ domain (*nu542* ΔPDZ) or those deleting EGL-19's c-terminal PDZ ligand (*nu496* ΔVTTL) were edited into the endogenous genes using CRISPR. These mutations significantly increased AP width, compared to WT controls. Sample sizes are as follows: WT (41), *shn-1(nu542)* (22), and *egl-19(nu496)* (22). Values that differ significantly from wild type controls are indicated (ns, not significant; *, $p < 0.05$; **, $p < 0.01$; ***, $p < 0.001$). Error bars indicate SEM.

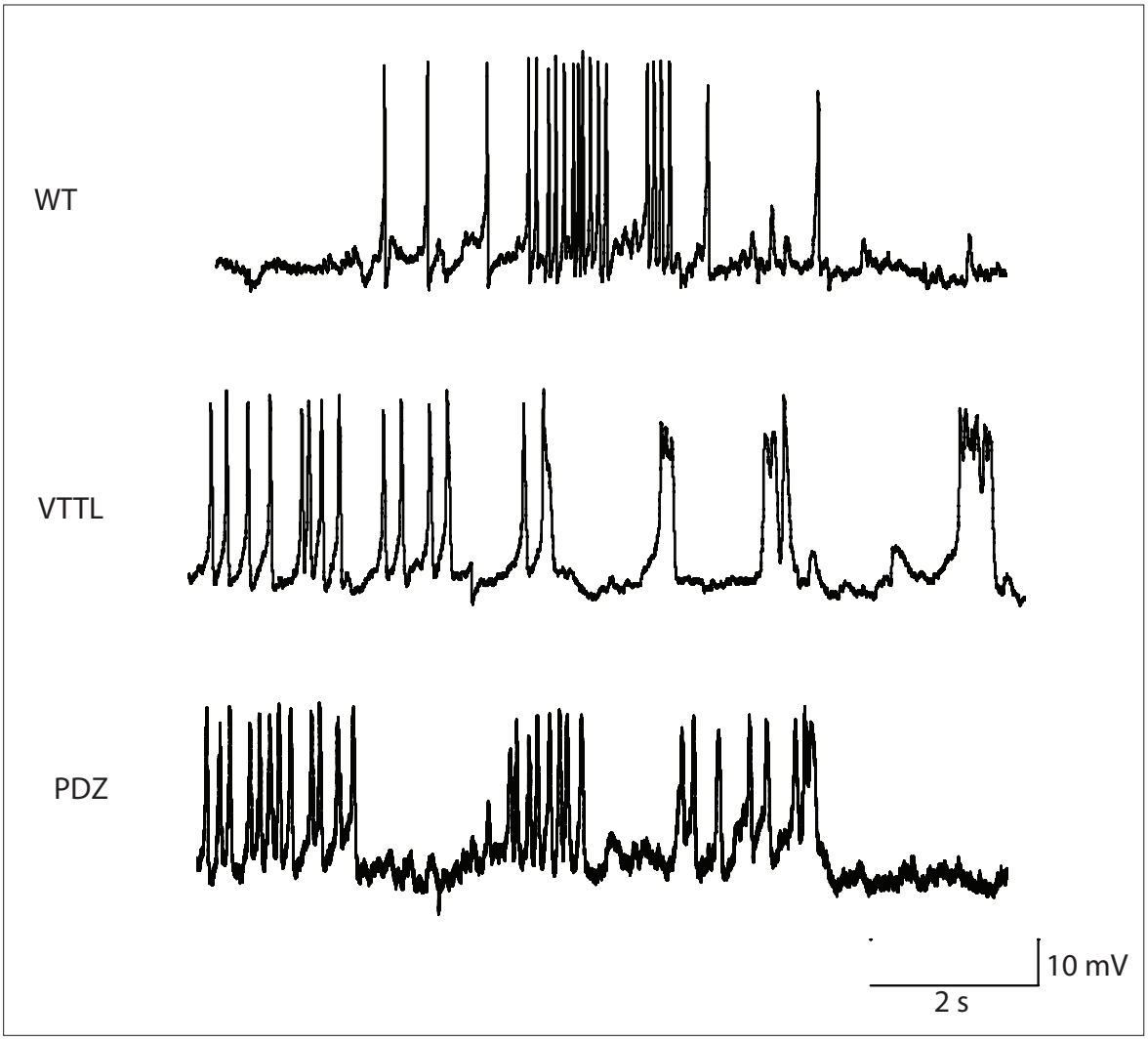

Figure 3—figure supplement 1. Representative traces for recordings summarized in ***Figure 3B and C***. Representative traces of spontaneous muscle APs are shown for the indicated genotypes.

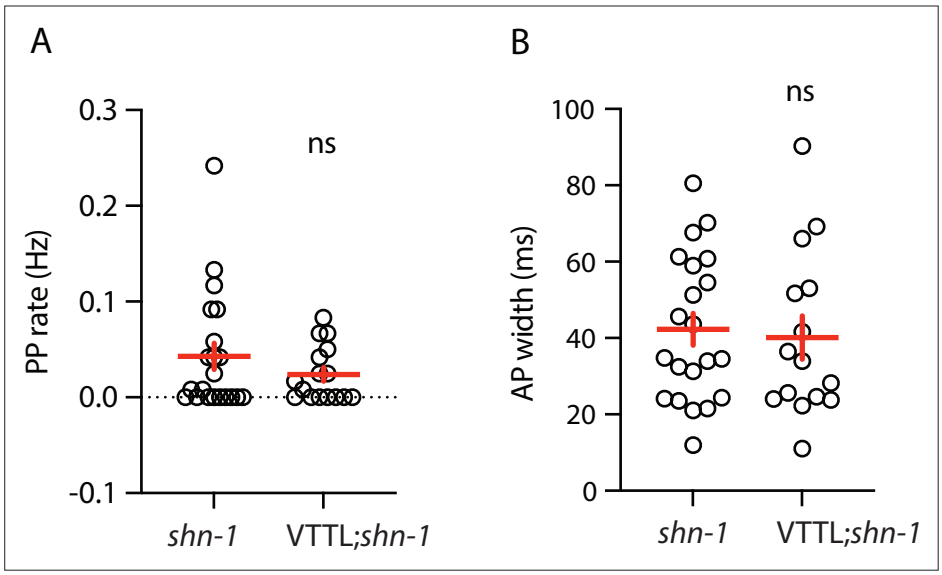

Figure 3—figure supplement 2. Muscle AP defects in *shn-1(null)* and *shn-1(null); egl-19*(ΔVTTL) double mutants are not significantly different. Mean PP rate and AP width are compared in the indicated genotypes. Sample sizes are as follows: *shn-1(nu712* null) (21); *shn-1(nu712); egl-19*(ΔVTTL) (15). Error bars indicate SEM. No significant differences were observed.

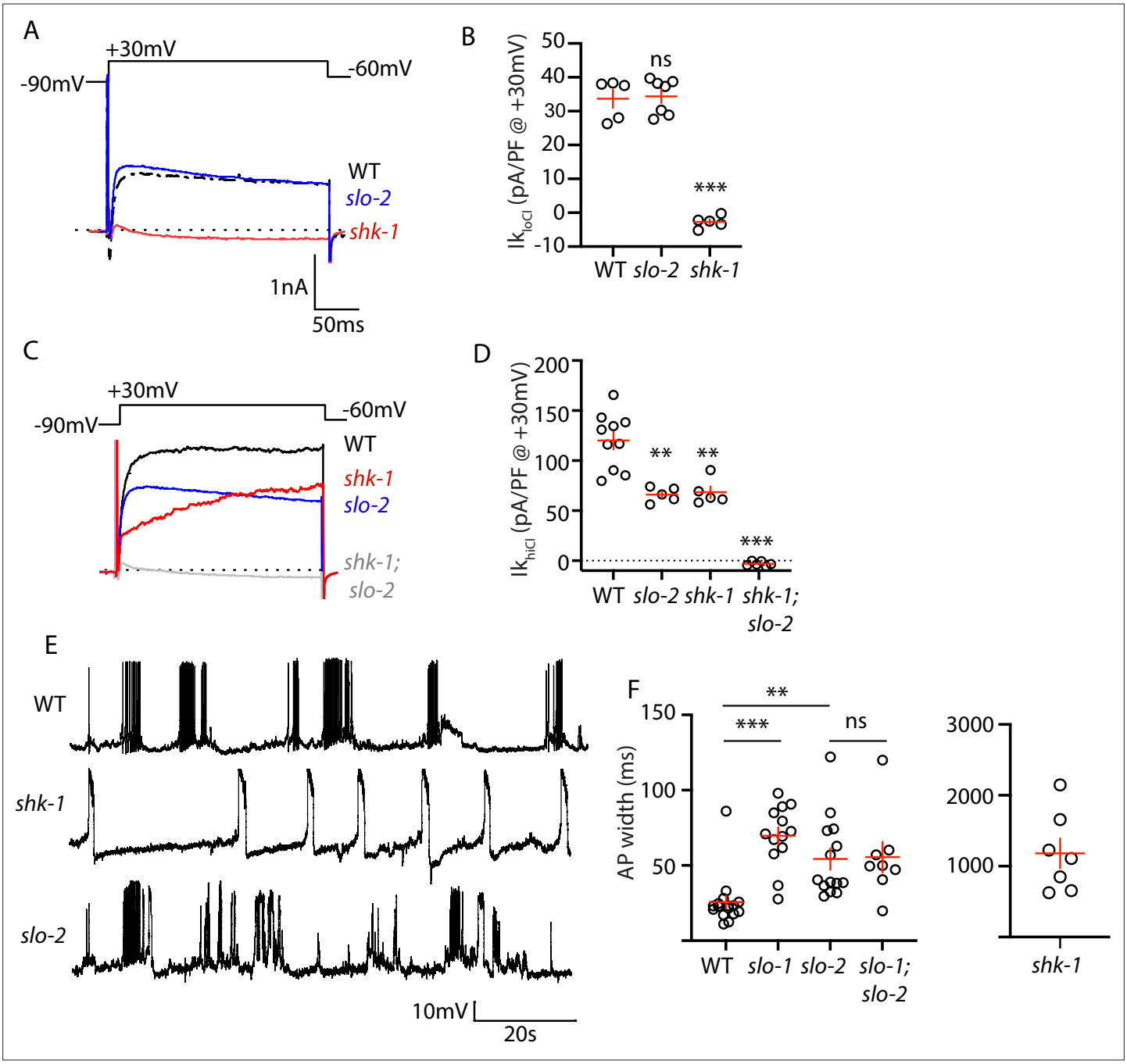

Figure 4. AP repolarization is mediated by SHK-1 and SLO channels. (**A–D**) Muscle voltage activated potassium currents are mediated by SHK-1 and SLO-2. Voltage activated potassium currents were recorded using pipette solutions containing low (Ik_{loCl}, **A–B**) and high (Ik_{hiCl}, **C–D**) chloride concentrations. Representative traces (**A,C**) and mean current density (**B,D**) at +30 mV are shown. Ik_{loCl} is mediated by SHK-1 whereas SHK-1 and SLO-2 equally contribute to Ik_{hiCl}. (**E–F**) AP durations are significantly increased in mutants lacking SHK-1, SLO-1, and SLO-2 channels. The AP widths observed in *slo-1; slo-2* double mutants were not significantly different from those found in *slo-2* single mutants. Representative traces (E and ***Figure 4—figure supplement 1***) and mean AP widths (**F**) are shown. Alleles used in this figure were: *shk-1(ok1581)*, *slo-1(js379)*, and *slo-2(nf100)*. Sample sizes are as follows: in panel B, WT (5), *slo-2* (7), and *shk-1* (5); in panel D, WT (10), *slo-2* (5), *shk-1* (5), *shk-1;slo-2* (6); in panel F, WT (16), *slo-1* (13), *slo-2* (14), *slo-1; slo-2* (8), *shk-1* (7). Values that differ significantly from wild type controls are indicated (ns, not significant; *, $p < 0.05$; **, $p < 0.01$; ***, $p < 0.001$). Error bars indicate SEM.

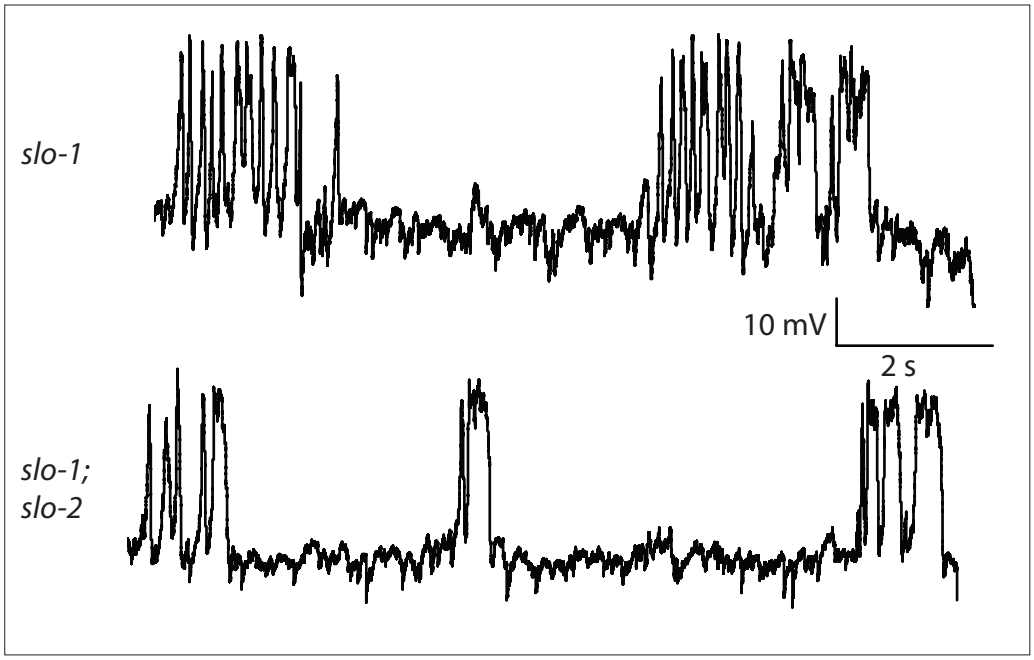

Figure 4—figure supplement 1. Representative traces for recordings summarized in ***Figure 4E***. Representative traces of spontaneous muscle APs are shown for the indicated genotypes.

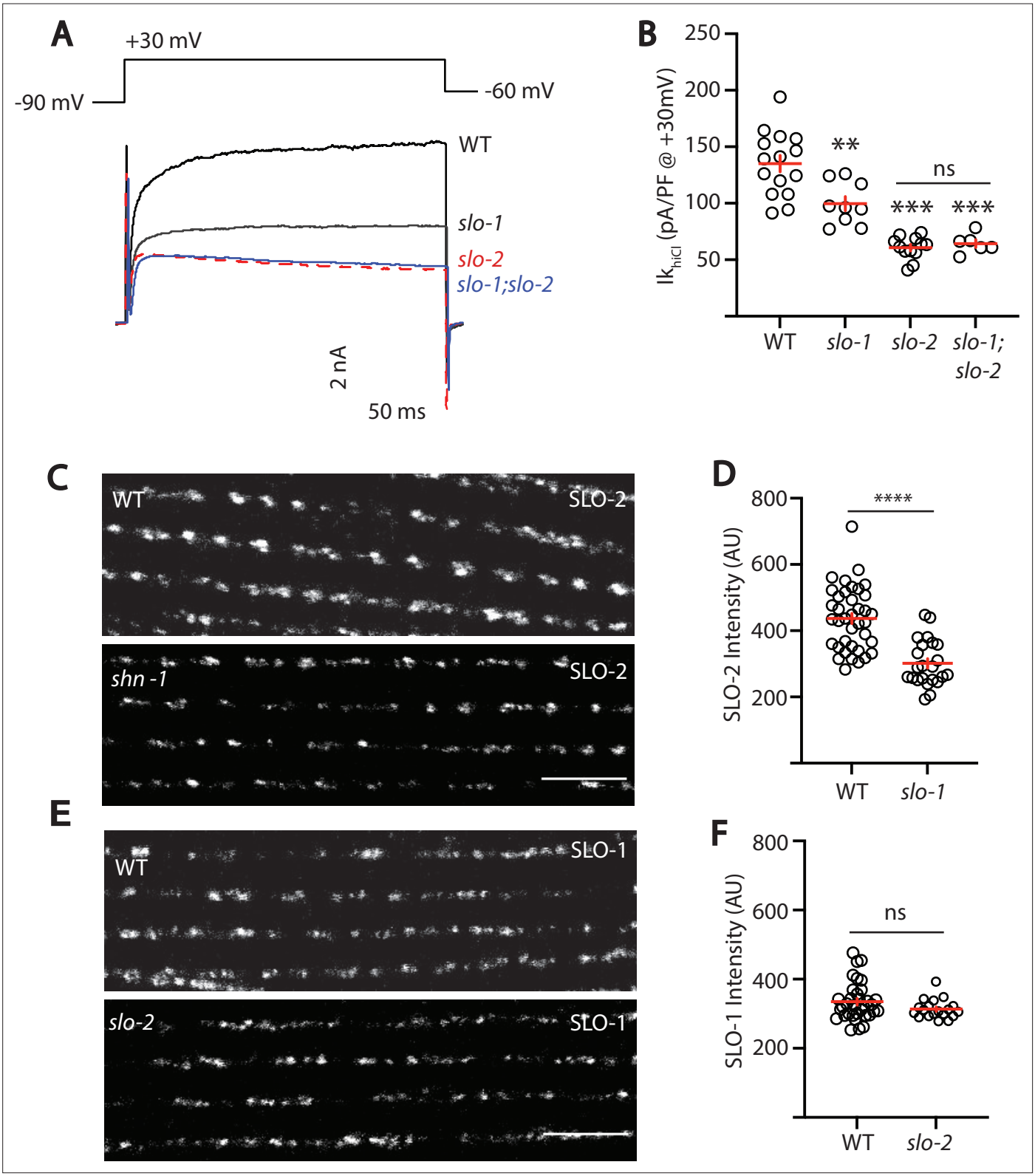

Figure 5. SLO-2 and SLO-1 function together in heteromeric channels. (**A–B**) Ik_{hiCl} was significantly decreased in *slo-1(js379)* and *slo-2(nf100)* single mutants but was not further decreased in *slo-1; slo-2* double mutants. Representative traces (**A**) and mean current density (**B**) at +30 mV are shown. Sample sizes for panel B: WT (15), *slo-1* (9), *slo-2* (12), *slo-1;slo-2* (6). (**C–F**) Expression of split GFP tagged SLO-2 (**C–D**) and SLO-1 (**E–F**) was analyzed in body muscles. CRISPR alleles were constructed adding 7 copies of GFP_{11} to the endogenous *slo-1* and *slo-2* genes (***Table 2***) and fluorescence was reconstituted by expressing GFP_{1-10} in body muscles. Controls showing that the GFP_{11} tags had no effect on AP width, RMP, and potassium currents are

Figure 5 continued on next page

Figure 5 continued

shown in ***Figure 5—figure supplement 1***. Representative images (**C and E**) and mean puncta intensity (**D and F**) are shown. SLO-2 puncta intensity was significantly decreased in *slo-1(js379)* mutants. SLO-1 puncta intensity was unaltered in *slo-2(nf100)* mutants. Sample sizes are as follows: in panel D, WT (38) and *slo-1* (23); in panel F, WT (34) and *slo-2* (19). Values that differ significantly from wild type controls are indicated (ns, not significant; *, $p < 0.05$; **, $p < 0.01$; ***, $p < 0.001$). Error bars indicate SEM. Scale bar indicates 4 μm.

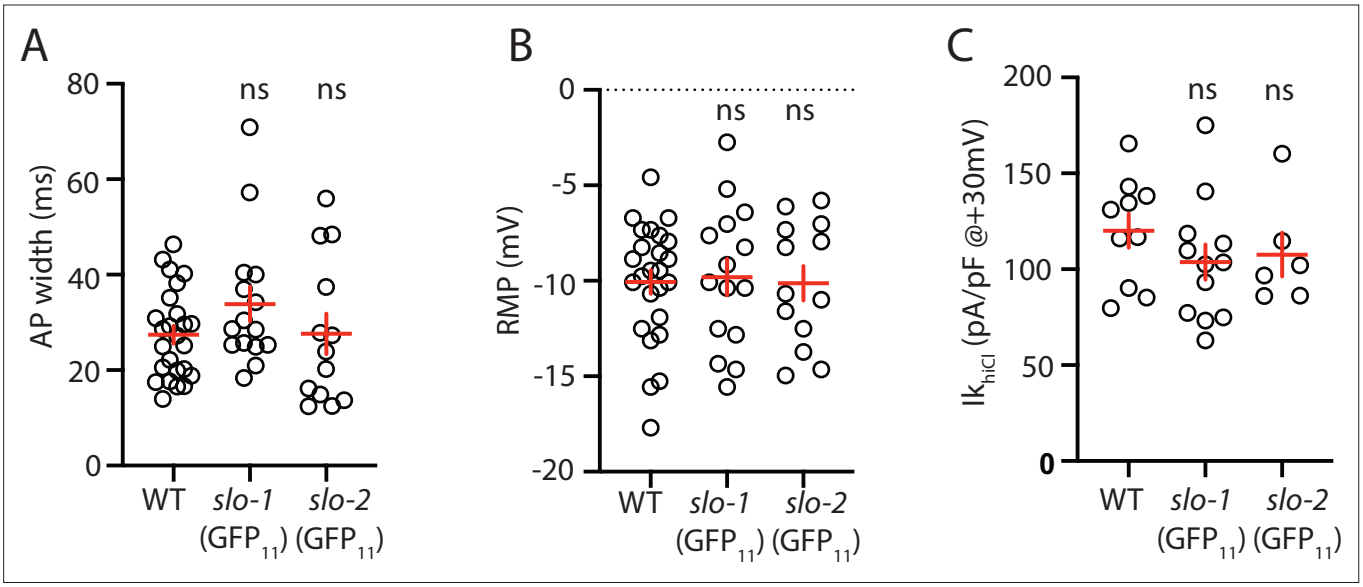

Figure 5—figure supplement 1. Analysis of GFP_{11} tagged *slo-1* and *slo-2* alleles. APs and potassium currents were analyzed in strains containing *slo-1(nu678* GFP_{11}) and *slo-2(nu725* GFP_{11}) together with the muscle>GFP_{1-10} transgene. Mean AP width (**A**), RMP (**B**), and Ik_{hiCl} current density (**C**) were not significantly different from WT controls. Sample sizes are as follows: in panels A and B, WT (25), *slo-1(nu678)* (15), and *slo-2(nu725)* (13); in panel C, WT (10), *slo-1(nu678)* (12), and *slo-2(nu725)* (6). Error bars indicate SEM.

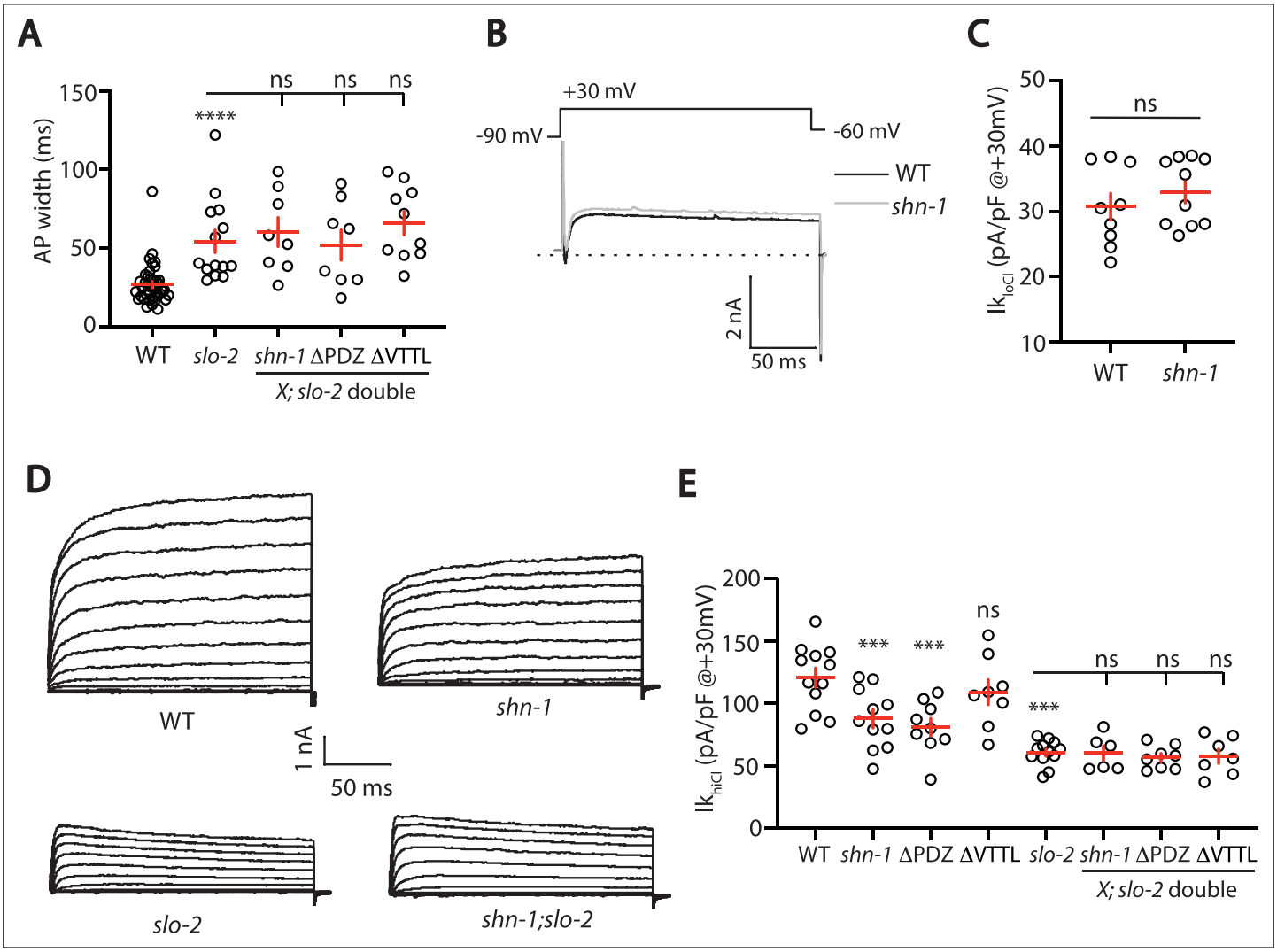

Figure 6. SHN-1 controls AP width by regulating SLO-2. (**A**) A *slo-2* null mutation blocks the effect of SHN-1 on AP width. Mean AP widths in *slo-2(nf100)* double mutants containing *shn-1(nu712* null), *shn-1(nu542* ΔPDZ), and *egl-19(nu496* ΔVTTL) mutations were not significantly different from those in *slo-2* single mutants. Representative traces are shown in ***Figure 6—figure supplement 1A***. Sample sizes: WT (41), *slo-2* (14), *slo-2;shn-1* (8), *slo-2;*ΔPDZ (8), and *slo-2;*ΔVTTL (10). (**B–C**) Ik_{loCl} currents were unaltered in *shn-1(nu712* null) mutants. Representative traces (**B**) and mean current density at +30 mV (**C**) are shown. Sample sizes: WT (9) and *shn-1* (10). These results show that SHK-1 channel function was unaffected in *shn-1* mutants. (**D–E**) Ik_{hiCl} currents were significantly smaller in *shn-1(nu712* null) and *shn-1(nu542* ΔPDZ) mutants but were unaffected in *egl-19(nu496* ΔVTTL) mutants. The effect of *shn-1* mutations on Ik_{hiCl} was eliminated in double mutants lacking SLO-2, indicating that the SHN-1 sensitive potassium current is mediated by SLO-2. Ik_{hiCl} currents were recorded from adult body wall muscles of the indicated genotypes at holding potentials of –60 to +60 mV. Representative traces (D and ***Figure 6—figure supplement 1B***) and mean current density at +30 mV (**E**) are shown. Sample sizes in panel E: WT (12), *shn-1* (11), *slo-2* (12), ΔPDZ (9), ΔVTTL (8), *slo-2;shn-1* (6), *slo-2;*ΔPDZ (8), and *slo-2;*ΔVTTL (7). Values that differ significantly from wild type controls are indicated (ns, not significant; *, $p < 0.05$; **, $p < 0.01$; ***, $p < 0.001$). Error bars indicate SEM.

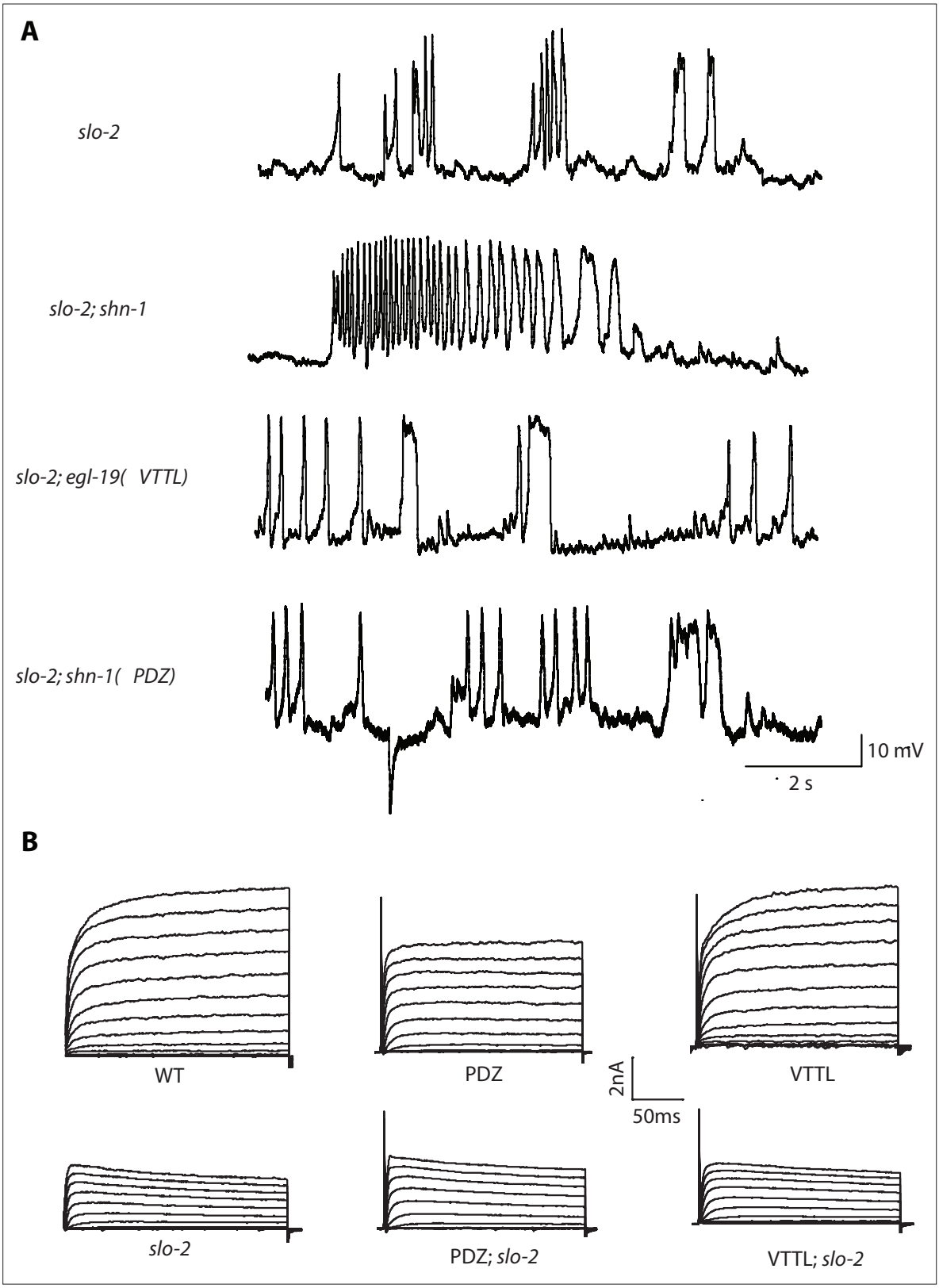

Figure 6—figure supplement 1. Representative traces for recordings summarized in ***Figure 6A and E***. Representative traces of spontaneous muscle APs (**A**) and Ik_{hiCl} currents at +30 mV (**B**) are shown for the indicated genotypes.

Figure 7. SHN-1 promotes EGL-19 to SLO-2 microdomain coupling. (**A–B**) SLO-2 activation is functionally coupled to EGL-19. Ik_{hiCl} was significantly reduced by nemadipine (an EGL-19 antagonist). This inhibitory effect of nemadipine on Ik_{hiCl} was eliminated in *slo-2(nf100)* mutants, indicating that the nemadipine sensitive current is mediated by SLO-2. Ik_{hiCl} currents were recorded from adult body wall muscles of the indicated genotypes at holding potentials of –60 to +60 mV. Representative Ik_{hiCl} traces (**A**) and mean current density as a function of membrane potential (**B**) are shown. (**C**) SLO-2

Figure 7 continued on next page

Figure 7 continued

activation requires microdomain coupling to EGL-19. Ik_{hiCl} currents recorded in BAPTA are significantly smaller than those in EGTA. The inhibitory effect of BAPTA was reduced in *shn-1(nu712* null) mutants and was eliminated in *slo-2(nf100*) mutants, indicating that the BAPTA sensitive current is mediated by SLO-2. The ratio of Ik_{hiCl} current density at +30 mV recorded in BAPTA to the mean current density recorded in EGTA is plotted for the indicated genotypes. Representative traces are shown in ***Figure 7—figure supplement 1A***. Sample sizes for panel C: WT (8), *slo-2* (8), and *shn-1* (10). (**D–E**) AP repolarization is mediated by microdomain activation of SLO-2. AP widths recorded in solutions containing BAPTA are wider than those recorded in EGTA. The effect of BAPTA on AP widths was reduced in *shn-1(nu712* null) mutants and was eliminated in *slo-2(nf100*) mutants, indicating that BAPTA's effect is mediated by SLO-2. Representative traces of WT muscle APs recorded in EGTA and BAPTA are shown (**D**). The ratio of AP widths recorded in BAPTA to the mean AP widths recorded in EGTA is plotted for the indicated genotypes (**E**). Representative traces for panel E are shown in ***Figure 7—figure supplement 1B***. Sample sizes for panel E: WT (8), *slo-2* (11), and *shn-1* (10). (**F–H**) SLO-2(nu725 GFP_{11}) is partially co-localized with EGL-19(nu722 $Cherry_{11}$) in body muscles. GFP_{11} and $Cherry_{11}$ fluorescence were reconstituted by expressing GFP_{1-10} and $Cherry_{1-10}$ in body muscles. SLO-2 puncta intensity was significantly reduced in *shn-1(nu712* null) mutants but was unaffected in *shn-1(nu542* ΔPDZ) and *egl-19(nu496* ΔVTTL) mutants. Representative images (**F**) and mean puncta intensity for SLO-2 (**G**) and EGL-19 (**H**) are shown. Sample sizes for panel G: *slo-2*(GFP_{11}) single mutants (38), and double mutants containing the *shn-1* (35), ΔPDZ (39), and ΔVTTL (18) mutations. Sample sizes for panel H: *egl-19*($Cherry_{11}$) single mutants (34) and *shn-1; egl-19*($Cherry_{11}$) double mutants (31). Values that differ significantly from wild type controls are indicated (ns, not significant; *, $p < 0.05$; **, $p < 0.01$; ***, $p < 0.001$). Error bars indicate SEM. Scale bar indicates 4 μm.

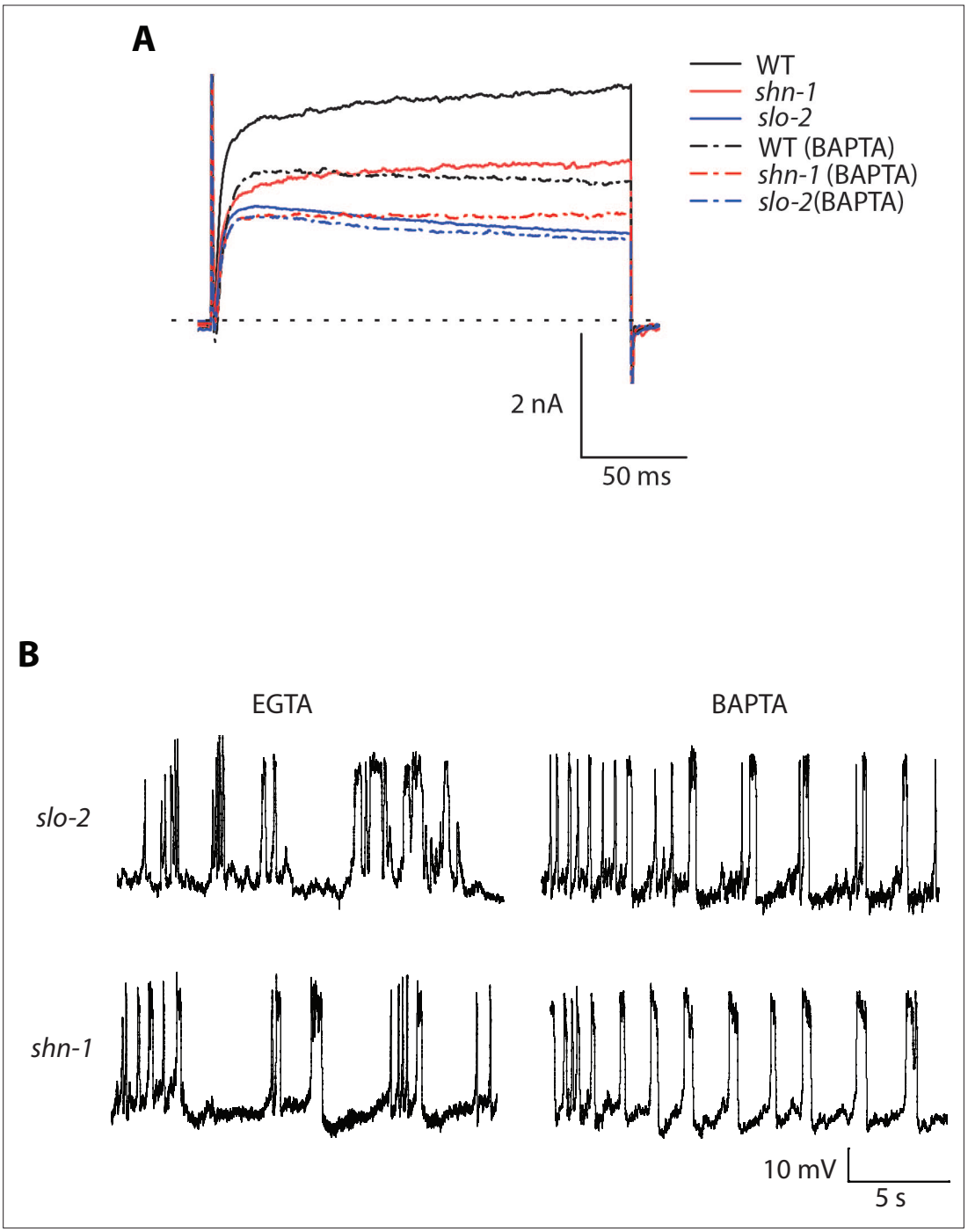

Figure 7—figure supplement 1. Representative traces for recordings summarized in ***Figure 7C and E***. Representative traces of Ik_{hiCl} currents at +30 mV (**A**) and spontaneous muscle APs (**B**) are shown for the indicated genotypes and recording conditions.

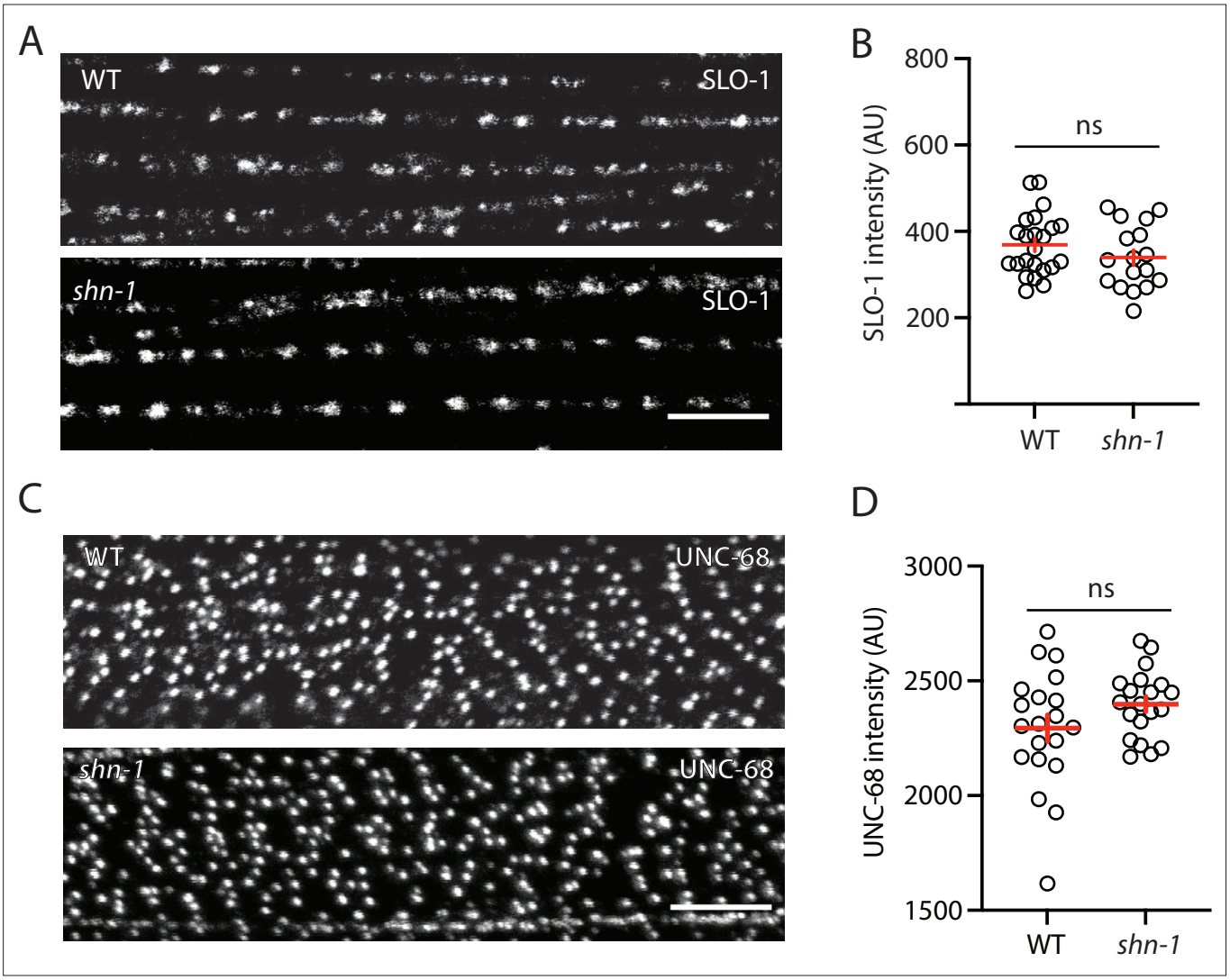

Figure 7—figure supplement 2. SLO-1 and UNC-68/RYR puncta intensity is unaltered in *shn-1* mutant muscles. SLO-1(nu678 GFP_{11}) and UNC-68(nu664 GFP_{11}) puncta intensity in body muscles is compared in WT and *shn-1*(null) mutants. GFP_{11} fluorescence was reconstituted by expressing GFP_{1-10} in body muscles. Representative images (**A and C**) and mean puncta intensity (**B and D**) are shown. Sample sizes: *slo-1*(GFP_{11}) single mutants (23); *shn-1(nu712* null)*;slo-1*(GFP_{11}) double mutants (17); *unc-68*(GFP_{11}) single mutants (20); and *shn-1(tm488* null)*;unc-68*(GFP_{11}) double mutants (20). No significant differences were observed. Error bars indicate SEM. Scale bars indicate 4 μm.

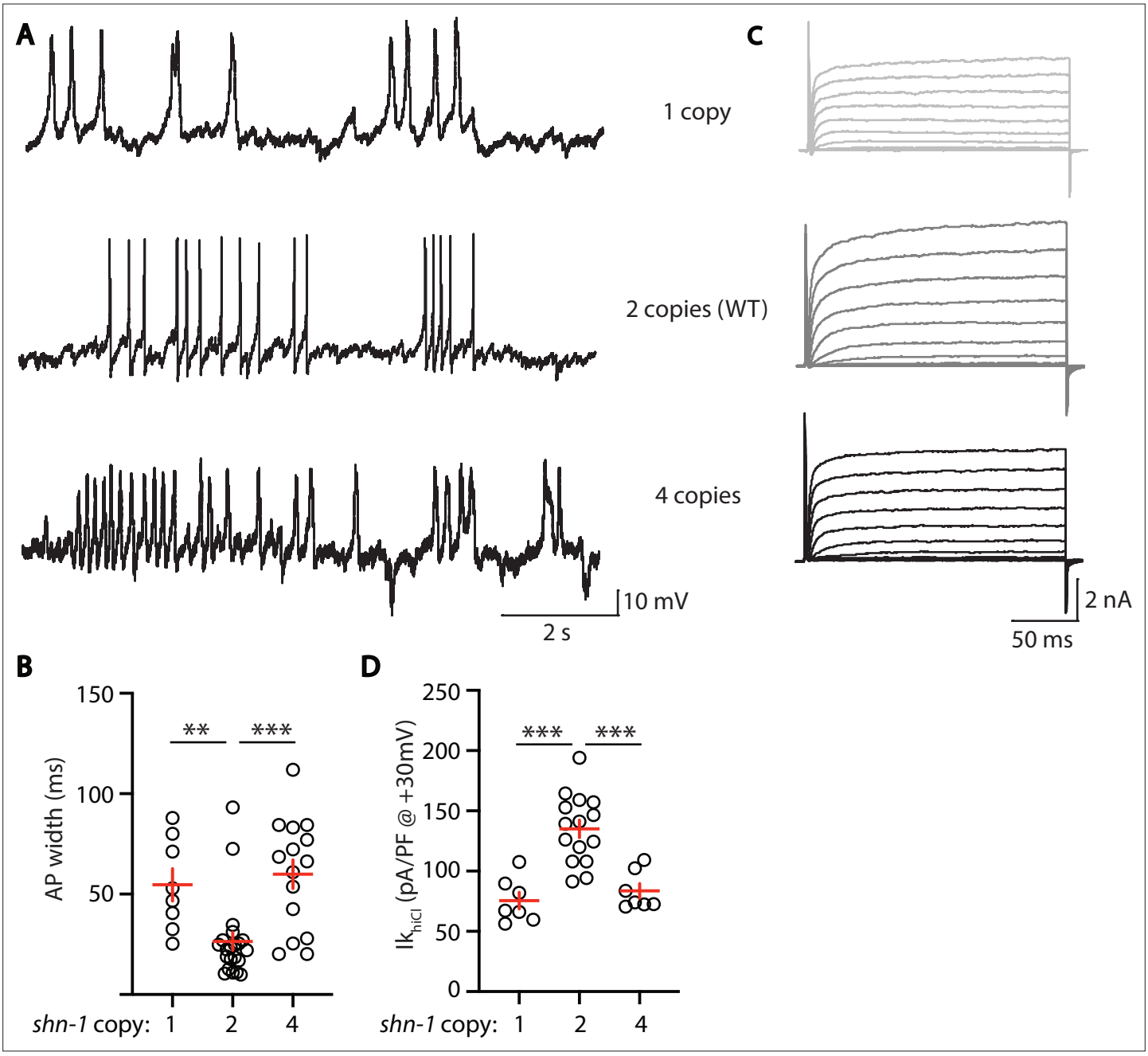

Figure 8. AP width and SLO-2 current are sensitive to *shn-1* gene dosage. The effect of *shn-1* gene dosage on AP widths (**A–B**) and Ik_{hiCl} current (**C–D**) was analyzed. Ik_{hiCl} was significantly decreased while AP duration was significantly increased in animals containing 1 and 4 copies of *shn-1* compared to WT controls (i.e. 2 copies). The following genotypes were analyzed: 1 copy of *shn-1* [*shn-1(nu712)*/ + heterozygotes], 2 copies of *shn-1* (WT) and 4 copies of *shn-1* (*nuSi26* homozygotes in wild-type). Ik_{hiCl} currents were recorded from adult body wall muscles of the indicated genotypes at holding potentials of –60 to +60 mV. Representative traces (**A,C**), mean AP width (**B**), and mean Ik_{hiCl} current density at +30 mV (**D**) are shown. Sample sizes: for panel B, 1 copy (8), 2 copies (21), and four copies (15); for panel D, 1 copy (8), 2 copies (15), and four copies (7). Significant differences are indicated (ns, not significant; *, $p < 0.05$; **, $p < 0.01$; ***, $p < 0.001$). Error bars indicate SEM.

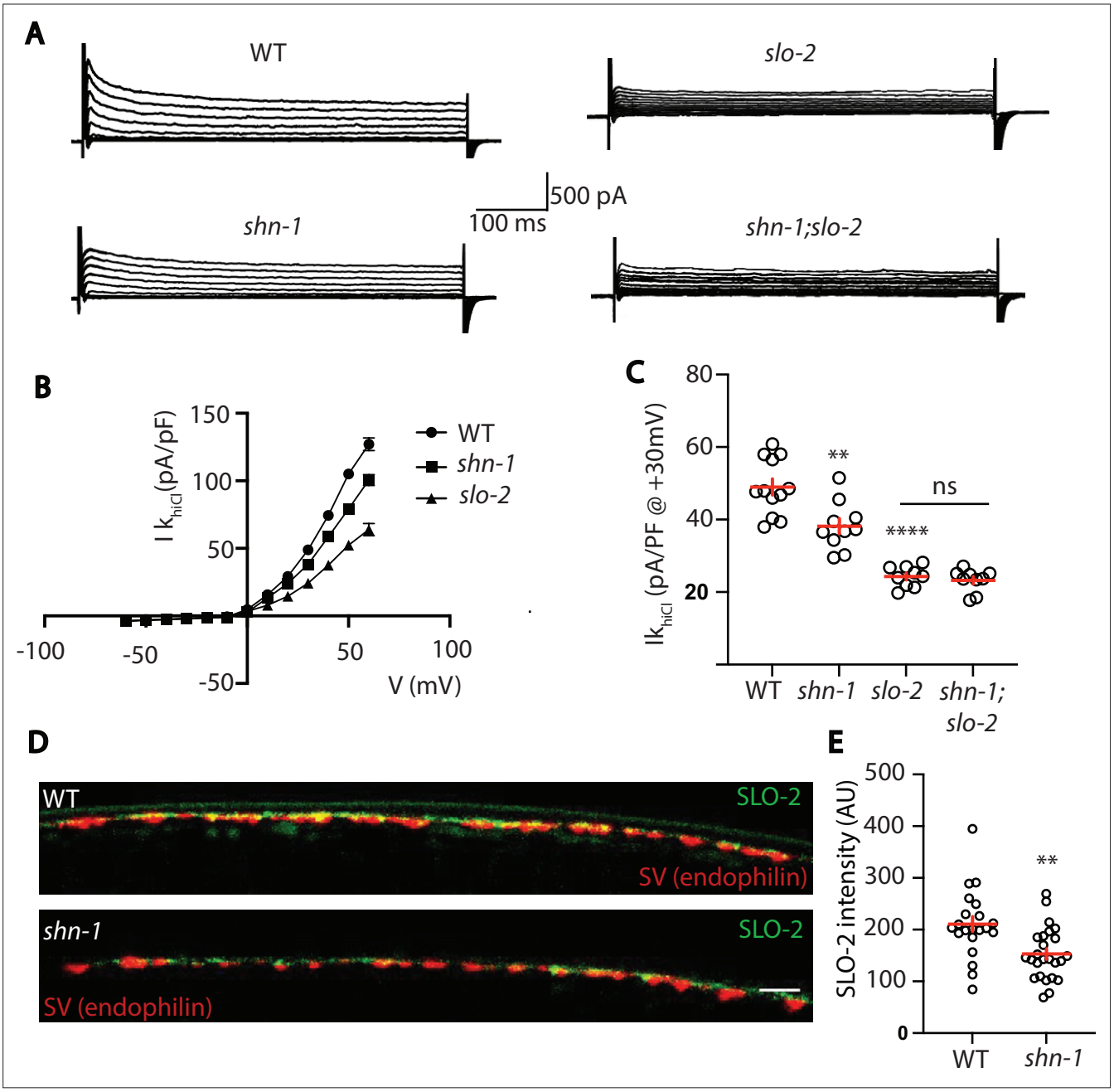

Figure 9. SHN-1 controls SLO-2 currents in motor neurons. (**A–B**) Ik_{hiCl} currents in cholinergic motor neurons were significantly decreased in *shn-1(nu712* null) mutants. Ik_{hiCl} currents were recorded from adult cholinergic motor neurons of the indicated genotypes at holding potentials of –60 to +60 mV. Representative traces (**A**), mean current density as a function of membrane potential (**B**), and mean current density at +30 mV (**C**) are shown. Sample sizes for panels B and C: WT (12), *shn-1* (10), *slo-2* (9), and *shn-1; slo-2* (9). (**D–E**) SLO-2 puncta intensity in motor neuron axons was significantly decreased in *shn-1(nu712* null) mutants. Representative images of SLO-2(*nu725* GFP_{11}) and a synaptic vesicle marker [UNC-57/Endophilin(mCherry)] in dorsal cord axons of DA/DB motor neurons are shown (**D**). GFP_{11} fluorescence was reconstituted with GFP_{1-10} expressed in DA/DB motor neurons (using the *unc-129* promoter). Mean SLO-2 puncta intensity in axons is plotted (**E**). Sample sizes for panel E: WT (21) and *shn-1* (25). Values that differ significantly from wild type controls are indicated (ns, not significant; *, $p < 0.05$; **, $p < 0.01$; ***, $p < 0.001$). Error bars indicate SEM. Scale bar indicates 2 μm.